Pergamon

J. Mech. Phys. Solids, Vol. 45, No. 5, pp. 709–729, 1997

0022–5096/97 $17.00 + 0.00

PII: S0022–5096(96)00107–X

SHAPE CHANGE OF A PORE IN A STRESSED SOLID VIA SURFACE DIFFUSION MOTIVATED BY SURFACE AND ELASTIC ENERGY VARIATION

WEIQING WANG† and Z. SUO‡

Mechanical and Environmental Engineering Department, Materials Department, University of California, Santa Barbara, CA 93106, U.S.A.

(*Received* 15 *July* 1996; *in revised form* 2 *October* 1996)

ABSTRACT

When a solid is stressed at a high temperature, atoms may move along various paths, causing a pore pre-existing in the solid to change shape. This paper assumes that atoms only diffuse on the pore surface and the solid is elastic. Both surface energy and elastic energy vary as the pore changes shape. When the surface energy variation dominates, the pore evolves to an equilibrium shape close to an ellipse. When the elastic energy variation dominates, the pore never reaches equilibrium; noses emerge and sharpen into crack tips. We describe the pore shape with a conformal mapping of many terms, determine the elastic field by a complex variable method, and evolve the mapping coefficients (and thereby the pore shape) by a set of ordinary differential equations. The numerical simulation gives the threshold for the shape instability, the time for a supercritical pore to grow crack tips, and the crack size when it just forms. Also explored are the effects of the applied stress state and surface tension anisotropy. We discuss the implications of the results for the lifetime of crystals stressed at elevated temperatures.

Keywords: A. surface diffusion, A. crack nucleation, B. elastic material, C. conformal mapping, C. Galerkin method.

1. INTRODUCTION

This work is motivated by two lines of studies. The first is on the strength of sapphire (single crystal aluminum oxide) fibers in a certain range of elevated temperatures. Newcomb and Tressler (1993) tested the fibers in tension at low loading rates at temperatures between 800 and 1500°C. The fibers did not creep, but the lifetime and the strength varied with loading rate and temperature. Prior to the mechanical testing, micron-sized pores existed in the fibers. Inspections of the fracture surfaces showed that often a fiber broke by a crack initiated from one of the pores. At 1400 and 1500°C, a circular region surrounded the pore: inside the circle, the fracture surface was smooth, indicative of slow decohesion; outside, the fracture surface consisted of a mirror, hackles and cleavage facets, typical of fast fracture of sapphire. At 800–

† Present address: Alphatec USA, 400 Industrial Park Drive, P.O. Box 2301, Manteca, CA 95336, U.S.A.

‡ To whom all correspondence should be addressed.

1200°C, the circular region was too small to see in a scanning electron microscope. Several issues are unsettled. How did the pore form a crack front to initiate the process of slow decohesion? Did the pore spend more time to form a crack front, or did the crack front spend more time to extend, before fast fracture?

The second line of studies is on surface self-diffusion driven by combined surface and elastic energy variation. A stress, acting parallel to a flat surface of an elastic solid, motivates atoms to diffuse on the surface, and can cause the surface to undulate (Asaro and Tiller, 1972; Grinfeld, 1986; Srolovitz, 1989; Gao, 1991; Yacobson, 1993). The undulation can break a strained film into islands (Spencer *et al.*, 1991; Freund and Jonsdottir, 1993; Schowalter, 1996; Wong and Thouless, 1996), or form cracks running into the bulk of the solid (Chiu and Gao, 1993; Yang and Srolovitz, 1993). Similarly, a pore in an elastic solid can grow into a crack by surface diffusion when the applied stress exceeds a threshold (Stevens and Dutton, 1971; McCartney, 1977; Gao, 1992, 1995; Suo and Wang, 1994). The theory provides a possible mechanism for a pore to form a crack front. Its comparison with the Newcomb and Tressler experiment is encouraging but inconclusive (Sun *et al.*, 1994).

We set out in this work to calculate several quantities important to the total lifetime, hoping that critical experiments would be carried out in the future. The previous models assumed that the pore evolves as a sequence of simple shapes (e.g., ellipses), for which elasticity solutions are readily available. However, the works of Chiu and Gao (1993), and Yang and Srolovitz (1993) on an imperfect surface have shown that noses concentrate stresses and localize diffusion over a distance much shorter than the pore radius. To adequately simulate pore shape change, in this paper we describe the pore shape with a conformal mapping of many terms, and evolve the shape by determining the mapping coefficients as functions of time. Section 2 reviews the theory and discusses its relations to other theories and experimental observations, motivating the detailed calculations. Section 3 formulates the ordinary differential equations for the mapping coefficients. Section 4 solves the elastic field outside the pore by using a complex variable method. Section 5 discusses the results of the simulation.

2. THE THEORY

Figure 1 illustrates the cross-section of a cylindrical pore in an infinite elastic solid under biaxial stresses, $\sigma_1 > \sigma_2 \geqslant 0$. The energy on the pore surface, U_S, integrates the surface tension over the pore surface area. The energy in the bulk of the crystal, U_E, integrates the elastic energy density over the crystal volume. The free energy of the system, G, has three contributions: $G = U_S + U_E - \text{load} \times \text{displacement}$. Linear elasticity dictates that $2U_E = \text{load} \times \text{displacement}$. Consequently, the free energy of an elastic solid under constant load is

$$G = U_S - U_E. \tag{1}$$

Note that U_S is exceedingly small compared to U_E. However, it is the variations in the energies associated with the pore shape change, rather than their absolute values, that drive self-diffusion.

A pore changes shape to reduce its free energy G. Compare two crystals, one

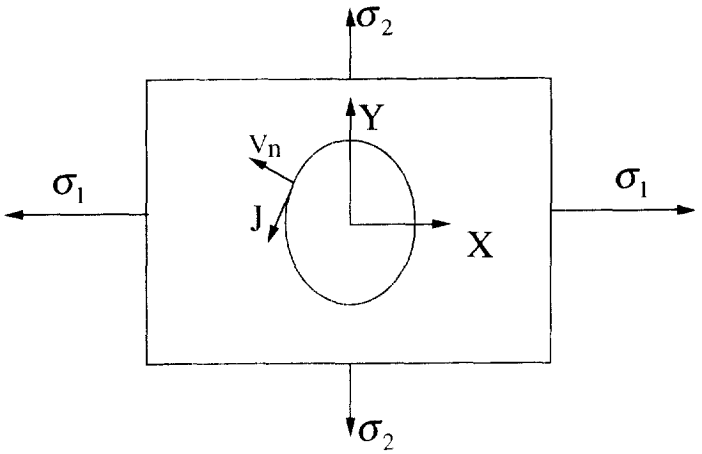

Fig. 1. The cross-section of a cylindrical pore in an infinite elastic solid under biaxial stresses. The pore changes shape as atoms diffuse on the surface, motivated by surface and elastic energy variation.

containing a circular pore, and the other a noncircular pore. The pores have the same volume (i.e., the same cross-sectional area of the cylinders). For simplicity assume that the surface tension is isotropic, and both crystals are under the same uniaxial stress σ_1. The noncircular pore elongates transverse to the direction of σ_1. Because the circle has the shortest perimeter among pores of the same cross-sectional area, the noncircular pore stores more surface energy than the circular pore. Because the crystal containing the noncircular pore has larger displacement at the loading point than the crystal containing the circular pore, the former stores more elastic energy than the latter. Consequently, the two energy variations compete to shape the pore: the surface tension favors the circular pore, and the applied stress favors the noncircular one.

Express the relative importance of the elastic and the surface energy variations with a dimensionless number

$$\Lambda = \frac{\sigma_1^2 R_0}{Y\gamma}, \tag{2}$$

where Y is Young's modulus, R_0 the initial circular pore radius, and γ the surface tension. This number will appear many times in this article to represent the loading level. Under no stress, the pore has a rounded shape maintained by the surface tension. When the crystal is under a uniaxial tensile stress, two behaviors are expected. If the applied stress is small (Λ small), the pore reaches an equilibrium shape close to an ellipse, compromising the stress and the surface tension. If the applied stress is large (Λ large), the pore can never reach equilibrium; noses emerge and sharpen into crack tips. Observe that this number takes the same form as that in the Griffith criterion. The length scale here, however, is the initial pore radius instead of a crack length. The two processes involve similar surface and elastic energy competition, but different processes: decohesion for a crack to advance, and diffusion for a pore to change shape.

To place this theory into perspective, recall other mass transport mechanisms by

which a pore evolves. At elevated temperatures, surface tension and stress may relocate mass by diffusion on a surface and a grain boundary, and by diffusion and creep in a crystal lattice. First consider diffusion on surfaces and boundaries. Hull and Rimmer (1959) and Chuang *et al.* (1979) showed that a pore on a grain boundary normal to an applied tensile stress grows as atoms diffuse from the pore surface into the grain boundary. Inserting one atom to the grain boundary, the tensile stress does work $\Omega\sigma$, where Ω is the volume per atom and σ the stress acting on, and normal to, the grain boundary. The elastic energy variation per atom relocation scales with $\Omega\sigma^2/Y$. As pointed out by Rice and Chuang (1981), when atoms are mobile on the grain boundary, and the grains can drift relative to each other to accommodate the space, the grain boundary does not have large stress concentration, and the elastic strain is small, say $\sigma/Y < 10^{-3}$. Consequently, the elastic energy variation is much smaller than the work done by the stress associated with the insertion of atoms, $\Omega\sigma^2/Y \ll \Omega\sigma$. The effect of elasticity of the grains is negligible: the models assume rigid grains. However, when the grain boundary is absent, or atoms are immobile on the grain boundary, the tensile stress cannot do work $\Omega\sigma$, and the elastic energy variation may become important.

Next consider a single crystal under a uniaxial tension. A pore in the crystal may change shape for several reasons. Elastic distortion causes small changes; large changes require mass transport. If the crystal creeps rapidly, the pore elongates in the loading direction (e.g., Budiansky *et al.*, 1982). Consequently, creep cannot be the dominant process in the Newcomb and Tressler experiments. If atoms diffuse rapidly on the pore surface and the crystal is elastic, as shown above, the pore elongates transverse to the loading direction.

On the basis of above considerations, we suggest the following sequence of events in the Newcomb and Tressler experiments. When the stress on the fiber exceeds a threshold, a pore pre-existing in the fiber changes shape to grow a crack front. After the crack front forms, its velocity is limited by a slow decohesion process. One may speculate on the possible mechanisms for the transition. For example, the surface tension can be substantially reduced by surface-adsorbing impurity atoms. When the pore is rounded, the mobile impurity atoms keep the surface tension low on the entire pore surface; the rate of pore shape change is limited by self-diffusion. After the crack front forms, the fresh surfaces are created by breaking atomic bonds; self-diffusion is unnecessary and does not limit the crack velocity, but impurity atoms transport to the crack front to reduce the surface tension of the freshly created surfaces, and thereby assist decohesion. Once the crack size is sufficiently large, the solid fractures instantaneously.

If this sequence of events did happen in the Newcomb and Tressler experiments, the fiber would spend its lifetime in two stages. In stage I, the pre-existing pores change shape by surface self-diffusion to sharpen the noses into crack tips. In stage II, the cracks extend by slow decohesion to attain the critical size for fast fracture. One stage may take much longer time than the other. In this connection, the micrographs can be deceptive. For the pore to form crack tips by self-diffusion, the overall geometric change may be small and difficult to see, as compared to the large area of slow decohesion. However, the time for the pore to form crack tips need not be shorter than the time for the crack to extend by decohesion. Such a time of little

overall geometric change (stage I) may well identify with the incubation time in an experimental observation. The two rate processes—self-diffusion and slow decohesion—have different temperature dependencies, which may be exploited in future experiments.

In the above, the pore shape change is attributed to surface self-diffusion, and slow decohesion to impurity transport. In reality, a pore may change shape by, for example, transport in a fluid phase in contact with the crystal, and slow decohesion may be limited by, for example, reaction at the crack tip. Also, the transition of the rate-limiting process from self-diffusion to impurity transport can occur before the crack tip forms. Nonetheless, to limit the scope of the calculations, this paper focuses on stage I, and assumes that surface self-diffusion is the only rate-limiting mechanism. The calculated results include the critical condition for a pore to grow a crack front, which corresponds to the threshold stress level below which the lifetime is infinite; the time needed for a pore to grow the crack, which is the stage I lifetime; and the size of the crack when it is just formed by surface diffusion, which would be an input to the calculation of the stage II lifetime.

3. THE DYNAMICAL SYSTEM

This section formulates the dynamics of the pore shape change. We use an approach developed by Wang *et al.* (1996) in a study of electromigration-induced transgranular slits. Most algebraic details are similar; here we only outline the main ideas. Readers interested in the simulation results may skip part of this section and all of the next.

3.1. *Geometry*

A pore lies on the (x, y) plane, or the complex z-plane, where $z = x + \mathrm{i}y$ and $\mathrm{i} = \sqrt{-1}$. On an auxiliary complex plane, ζ-plane, lies a unit circle, $\zeta = \exp(i\theta)$, $0 \leqslant \theta < 2\pi$. A power series,

$$z = \omega(\zeta) \equiv a_{-1}\zeta + \frac{a_1}{\zeta} + \frac{a_2}{\zeta^2} + \ldots + \frac{a_m}{\zeta^m}, \tag{3}$$

maps the unit circle on the ζ-plane to the pore on the z-plane. Choose $\omega(\zeta)$ to be an analytic function outside the unit circle—that is, choose the coefficients such that $\omega'(\zeta) \neq 0$ when $|\zeta| > 1$. According to the theory of conformal mapping, such an analytic function also maps the exterior of the unit circle on the ζ-plane to the exterior of the pore on the z-plane.

When the pore is symmetric with respect to the x-axis, all the mapping coefficients, $a_{-1}, a_1, a_2, \ldots, a_m$, are real numbers. When the pore is also symmetric with respect to the y-axis, $a_2 = a_4 = a_6 = \ldots = 0$. In the simulation, we took advantage of the first symmetry but not the second. The mapping coefficients describe the pore shape: the more terms the series contains, the more variety of pore shapes it can describe. When the pore changes shape, the unit circle on the ζ-plane remains fixed, but the mapping coefficients change. Consequently, the mapping coefficients, $a_{-1}, a_1, a_2, \ldots, a_m$, are the

generalized coordinates of this dynamical system, and their time rates, $\dot{a}_{-1}$, $\dot{a}_1$, $\dot{a}_2, \ldots, \dot{a}_m$, the generalized velocities.

Imagine that the pore shape changes slightly as a small amount of mass relocates along the surface. Describe the shape change with a set of small variations in the mapping coefficients, $\delta a_{-1}, \delta a_1, \delta a_2, \ldots, \delta a_m$. An element of the pore surface, ds, moves in the direction normal to the element by a small distance δr_n, which relates to the mapping coefficient variations. Let δI be the number of atoms crossing per unit length on the surface and ds be the curve element. Mass conservation requires that

$$\delta r_n = \Omega \frac{\partial(\delta I)}{\partial s}. \tag{4}$$

Integrating, we relate δI to the mapping coefficient variations:

$$\delta I = A_{-1}\delta a_{-1} + A_1 \delta a_1 + A_2 \delta a_2 + \ldots + A_m \delta a_m. \tag{5}$$

Here A_i are functions of θ and a_i, as listed in Wang *et al.* (1996).

Denote the surface velocity normal to the surface element by v_n, and the number of atoms per unit time crossing per unit length on the surface by J. Mass conservation requires that they satisfy a relation similar to (4), namely,

$$v_n = \Omega \frac{\partial J}{\partial s}. \tag{6}$$

Consequently, J relates to the generalized velocities in a way similar to (5):

$$J = A_{-1}\dot{a}_{-1} + A_1 \dot{a}_1 + A_2 \dot{a}_2 + \ldots + A_m \dot{a}_m. \tag{7}$$

3.2. *The weak statement*

Denote δG as the free energy variation associated with an arbitrary small change of the pore shape. Define the diffusion driving force, F, as the free energy reduction per atom moving per unit distance, namely,

$$\int F \delta I \, \mathrm{d}s = -\delta G. \tag{8}$$

The integral extends over the pore surface. We adopt a linear kinetic law, i.e., the flux is proportional to the driving force:

$$J = MF, \tag{9}$$

where M is the atomic mobility on the pore surface, and relates to the surface diffusivity by the Einstein relation, $M = D_s \delta_s / \Omega k T$, where D_s is the surface self-diffusivity, δ_s the thickness of atomic layers participating in surface diffusion, k Boltzmann's constant, and T the absolute temperature. Eliminating F from (8) and (9), we obtain

$$\int \frac{J \delta I}{M} \mathrm{d}s = -\delta G. \tag{10}$$

The flux J satisfies (10) for any arbitrary small pore shape change. This is the weak statement of the dynamical system.

3.3. *Ordinary differential equations governing the mapping coefficients*

We next follow the Galerkin procedure to transform the weak statement to a set of ordinary differential equations. The free energy of the system is a function of the mapping coefficients, $G(a_{-1}, a_1, a_2, \ldots)$. Its variation is linear in the variations of the mapping coefficients, namely,

$$\delta G = -f_{-1}\delta a_{-1} - f_1\delta a_1 - f_2\delta a_2 - \ldots - f_m\delta a_m. \tag{11}$$

The generalized forces, f_i, are the differential coefficients of the free energy:

$$f_i = -\partial G/\partial a_i. \tag{12}$$

Substituting (5), (7) and (11) into (10), and noting that $\delta a_{-1}, \delta a_1, \delta a_2, \ldots, \delta a_m$ can each vary independently, we obtain that

$$\sum_k H_{ik}\dot{a}_k = f_i, \tag{13}$$

with the generalized viscosities being

$$H_{ik} = \int \frac{A_i A_k}{M}\,\mathrm{d}s. \tag{14}$$

The viscosity matrix $[H_{ik}]$ is symmetric and positive-definite. Both the force column and the viscosity matrix depend on the mapping coefficients. Consequently, (13) is a set of nonlinear ordinary differential equations that evolve the mapping coefficients. We enforce pore area conservation with a Lagrange multiplier, and integrate the ordinary differential equations with a standard computer routine.

4. ELASTIC FIELD AROUND A PORE

4.1. *Complex functions*

This section determines the elastic field around a pore in an infinite elastic solid under remote stresses (Fig. 1). For the two-dimensional elasticity field, it is well known that the stresses, the displacements, and the resultant forces on an arc relate to two analytic functions, $\phi(z)$ and $\psi(z)$, namely,

$$\frac{\sigma_{22}+\sigma_{11}}{2} = \phi'(z) + \bar{\phi}'(\bar{z}), \tag{15a}$$

$$\frac{\sigma_{22}-\sigma_{11}}{2} + \mathrm{i}\sigma_{12} = \bar{z}\phi''(z) + \psi'(z), \tag{15b}$$

$$\frac{Y}{1+\nu}(u_1 + \mathrm{i}u_2) = \kappa\phi(z) - z\bar{\phi}'(\bar{z}) - \bar{\psi}(\bar{z}), \tag{15c}$$

$$F_1 + \mathrm{i}F_2 = -\mathrm{i}[\phi(z) + z\bar{\phi}'(\bar{z}) + \bar{\psi}(\bar{z})], \tag{15d}$$

where $\kappa = (3-\nu)/(1+\nu)$ for plane stress and $\kappa = 3-4\nu$ the plane strain, with ν being Poisson's ratio.

The two analytic functions depend on boundary conditions. They are also analytic on the ζ-plane outside the unit circle. Expand them in power series:

$$\phi(\zeta) = b_{-1}\zeta + \frac{b_1}{\zeta} + \frac{b_2}{\zeta^2} + \ldots \tag{16}$$

$$\psi(\zeta) = c_{-1}\zeta + \frac{c_1}{\zeta} + \frac{c_2}{\zeta^2} + \ldots. \tag{17}$$

The number of terms in each will soon be determined. The leading coefficients depend on the stresses applied remote from the pore:

$$b_{-1} = a_{-1}(\sigma_2 + \sigma_1)/4, \quad c_{-1} = a_{-1}(\sigma_2 - \sigma_1)/2. \tag{18}$$

All the coefficients, b_i and c_i, are real numbers for the present problem.

Let α be a point on the unit circle in the ζ-plane. The pore surface is traction-free, and (15d) requires that

$$\phi(\alpha) + \frac{\omega(\alpha)}{\bar{\omega}'(\bar{\alpha})}\bar{\phi}'(\bar{\alpha}) + \bar{\psi}(\bar{\alpha}) = 0. \tag{19}$$

Noting that $\bar{\alpha} = 1/\alpha$ and all the power series have real coefficients, the above becomes

$$\alpha^m \phi(\alpha) = -\frac{\alpha^m \omega(\alpha)}{\omega'\left(\frac{1}{\alpha}\right)}\phi'\left(\frac{1}{\alpha}\right) - \alpha^m \psi\left(\frac{1}{\alpha}\right). \tag{20}$$

The right-hand side is an analytic function inside the unit circle, and the left-hand side an analytic function outside the unit circle. Equation (20) states that the two analytic functions are equal on the circle. Consequently, a function analytic on the entire ζ-plane, namely, a polynomial $P(\zeta)$, exists, which equals the two functions on either side of the circle. Thus,

$$P(\zeta) = \begin{cases} \zeta^m \phi(\zeta), & |\zeta| > 1 \\ -\dfrac{\zeta^m \omega(\zeta)}{\omega'\left(\frac{1}{\zeta}\right)}\phi'\left(\dfrac{1}{\zeta}\right) - \zeta^m \psi\left(\dfrac{1}{\zeta}\right), & |\zeta| < 1. \end{cases} \tag{21}$$

A comparison of the first equation in the above and the asymptotic form (16) dictates that the polynomial $P(\zeta)$ be of order $m+1$, namely,

$$P(\zeta) = b_{-1}\zeta^{m+1} + b_1\zeta^{m-1} + b_2\zeta^{m-2} + \ldots + b_m\zeta^0.$$

Consequently, the power series of $\phi(z)$ contains terms up to b_m.

Write the second equation in (21) as

$$(a_{-1} - a_1\zeta^2 - 2a_2\zeta^3 - \ldots - ma_m\zeta^{m+1})(b_{-1}\zeta^{m-1} + b_1\zeta^{m-1} + b_2\zeta^{m-2} + \ldots + b_m)$$
$$+ (a_{-1}\zeta^{m-1} + a_1\zeta^{m-1} + a_2\zeta^{m-2} + \ldots + a_m)(b_{-1} - b_1\zeta^2 - 2b_2\zeta^3 - \ldots - mb_m\zeta^{m+1})$$

$$+(a_{-1}-a_1\zeta^2-2a_2\zeta^3-\ldots-ma_m\zeta^{m+1})(c_{-1}\zeta^{m-1}+c_1\zeta^{m+1}+c_2\zeta^{m+2}+\ldots)=0.$$

Compare the coefficients, and one obtains

$$\zeta^0: \quad a_{-1}b_m+b_{-1}a_m=0$$

$$\zeta^1: \quad a_{-1}b_{m-1}+b_{-1}a_{m-1}=0$$

$$\zeta^2: \quad a_{-1}b_{m-2}-a_1b_m+b_{-1}a_{m-2}-a_mb_1=0$$

$$\zeta^3: \quad a_{-1}b_{m-3}-a_1b_{m-1}-2a_2b_m+b_{-1}a_{m-3}-2a_mb_2-a_{m-1}b_1=0$$

$$\ldots$$

$$\zeta^{m-2}: \quad [a_{-1}b_2-a_1b_4-\ldots-(m-3)a_{m-3}b_m]$$
$$+[b_{-1}a_2-b_1a_4-\ldots-(m-3)b_{m-3}a_m]=0$$

$$\zeta^{m-1}: \quad [a_{-1}b_1-a_1b_3-\ldots-(m-2)a_{m-2}b_m]$$
$$+[b_{-1}a_1-b_1a_3-\ldots-(m-2)b_{m-2}a_m]+c_{-1}a_{-1}=0.$$

Regarding the mapping coefficients a_i as known, the above is a set of m linear algebraic equations for $b_1, b_2, \ldots, b_m$. Once they are solved, so is $\phi(\zeta)$. The other function is determined by

$$\psi(\zeta)=-\phi\left(\frac{1}{\zeta}\right)-\omega\left(\frac{1}{\zeta}\right)\frac{\phi'(\zeta)}{\omega'(\zeta)}. \tag{22}$$

4.2. *Elastic energy*

For an elastic body with a traction-free pore, the remote stresses store elastic energy (Suo and Wang, 1994).

$$U_1=U_0+\tfrac{1}{2}\int\sigma_{ij}n_iu_j\,\mathrm{d}s. \tag{23}$$

Here U_0 is independent of the pore geometry, and therefore does not affect the pore dynamics; only the second term need be included in the free energy G. The integral is over the pore surface, where σ_{ij} are the applied stresses, n_i the unit normal vector of the pore surface pointing into the solid, and u_j the displacements on the pore surface.

The displacement on the pore surface is computed from (15c), which, together with the traction-free condition, gives

$$u_1+\mathrm{i}u_2=\frac{4}{Y}\phi(z), \tag{24}$$

under the plane stress conditions. Under the plane strain conditions, Y should be replaced by $Y/(1-\nu^2)$.

Noticing $n_1=\mathrm{d}y/\mathrm{d}s$ and $n_2=-\mathrm{d}x/\mathrm{d}s$, we rewrite the integral in (23) as

$$\frac{\sigma_1+\sigma_2}{4}\,\mathrm{Im}\,[\int(u_1-\mathrm{i}u_2)\,\mathrm{d}z]+\frac{\sigma_1-\sigma_2}{4}\,\mathrm{Im}\,[\int(u_1+\mathrm{i}u_2)\,\mathrm{d}z].$$

Here Im[ ] stands for the imaginary part of a complex number. Carrying out the contour integrals,

$$\int \bar{\phi}(\bar{z})\,\mathrm{d}z = \int \phi\left(\frac{1}{\zeta}\right)\omega'(\zeta)\,\mathrm{d}\zeta$$

$$= \int \left(\frac{b_{-1}}{\zeta} + b_1\zeta + b_2\zeta^2 + \ldots b_m\zeta^m\right)\left(a_{-1} - \frac{a_1}{\zeta^2} - \frac{2a_2}{\zeta^3} - \ldots - \frac{ma_m}{\zeta^{m+1}}\right)\mathrm{d}\zeta$$

$$= 2\pi\mathrm{i}(b_{-1}a_{-1} - a_1b_1 - 2a_2b_2 - \ldots - ma_mb_m)$$

and

$$\int \phi(z)\,\mathrm{d}z = \int \phi(\zeta)\omega'(\zeta)\,\mathrm{d}\zeta$$

$$= \int \left(b_{-1}\zeta + \frac{b_1}{\zeta} + \frac{b_2}{\zeta^2} + \ldots + \frac{b_m}{\zeta^m}\right)\left(a_{-1} - \frac{a_1}{\zeta^2} - \frac{2a_2}{\zeta^3} - \ldots - \frac{ma_m}{\zeta^{m+1}}\right)\mathrm{d}\zeta$$

$$= 2\pi\mathrm{i}(a_{-1}b_1 - b_{-1}a_1)$$

the integral in (23) becomes

$$\frac{2\pi(\sigma_1+\sigma_2)}{Y}(b_{-1}a_{-1} - a_1b_1 - 2a_2b_2 - \ldots - ma_mb_m) + \frac{2\pi(\sigma_1-\sigma_2)}{Y}(a_{-1}b_1 - b_{-1}a_1). \tag{25}$$

Because $b_1, b_2, \ldots, b_m$ relate to $a_{-1}, a_1, a_2, \ldots, a_m$, the elastic energy of the system is a function of the mapping coefficients, as expected.

5. SIMULATION RESULTS AND DISCUSSION

When a circular pore in an isotropic solid is under equal biaxial stresses, $\sigma_1 = \sigma_2$, no driving force motivates atoms to diffuse on the pore surface, and the pore is in an equilibrium state. However, the studies cited in Section 1 have shown that the pore is unstable when $\Lambda > 3/8$—that is, an imperfection can cause the pore to change shape. In this simulation, we started with a circular pore in a crystal under unequal biaxial stresses, $\sigma_1 > \sigma_2$. The surface tension was taken to be isotropic except in the last subsection. The results shown here were computed with 15 terms in the conformal mapping. We varied the number of terms to ensure that the results are insensitive to the variation.

5.1. *Threshold*

Figure 2 shows the sequences of two evolving pores. Each is subject to a uniaxial stress in the horizontal direction, $\Lambda = 0.25$ for the pore on the left column, and $\Lambda = 0.6$ on the right. The time is given in units of a characteristic time scale.

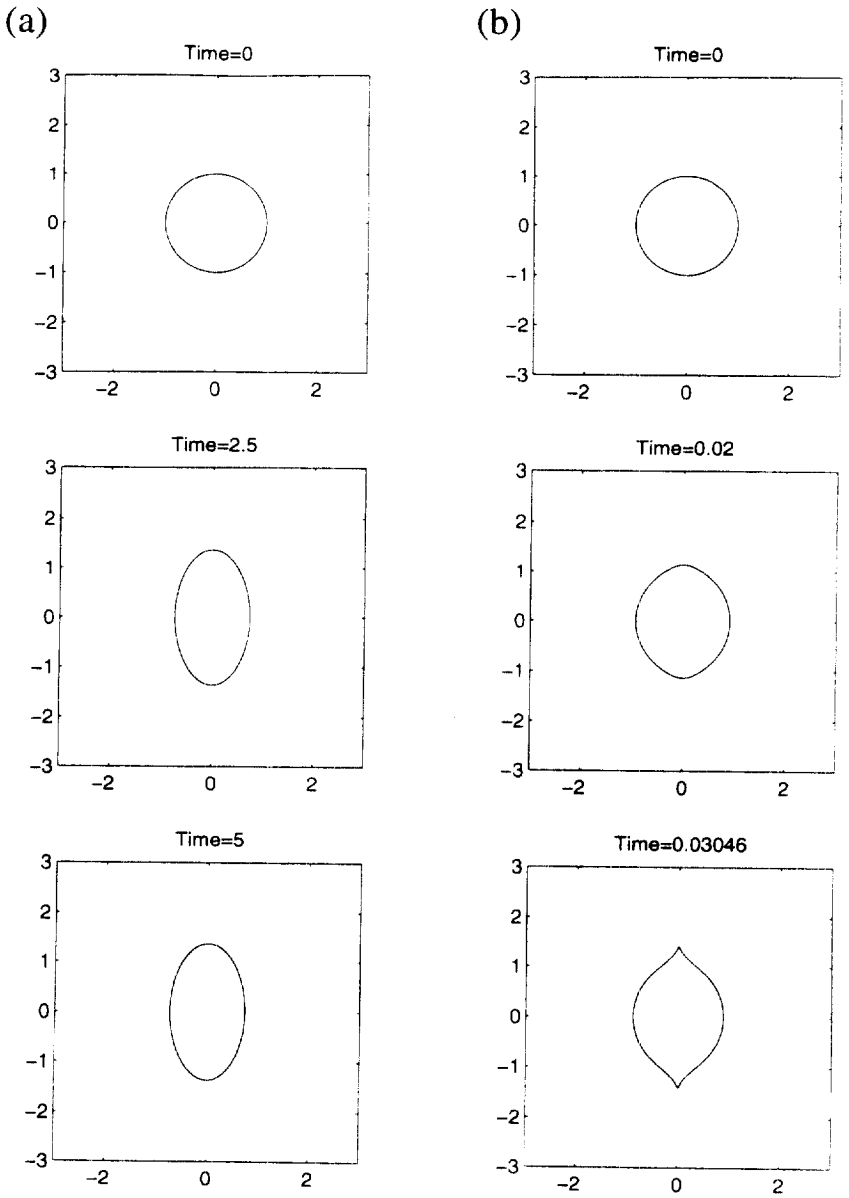

Fig. 2. Two sequences of evolving pores under uniaxial stress σ_1. The sequence on the left is a pore under $\Lambda = 0.25$; on the right, $\Lambda = 0.6$.

$$\tau_0 = \frac{R_0^4}{\Omega^2 M\gamma}. \tag{26}$$

When Λ is small, the surface energy variation dominates, and the pore reaches an equilibrium shape close to an ellipse; the pore does not grow crack tips. When Λ is

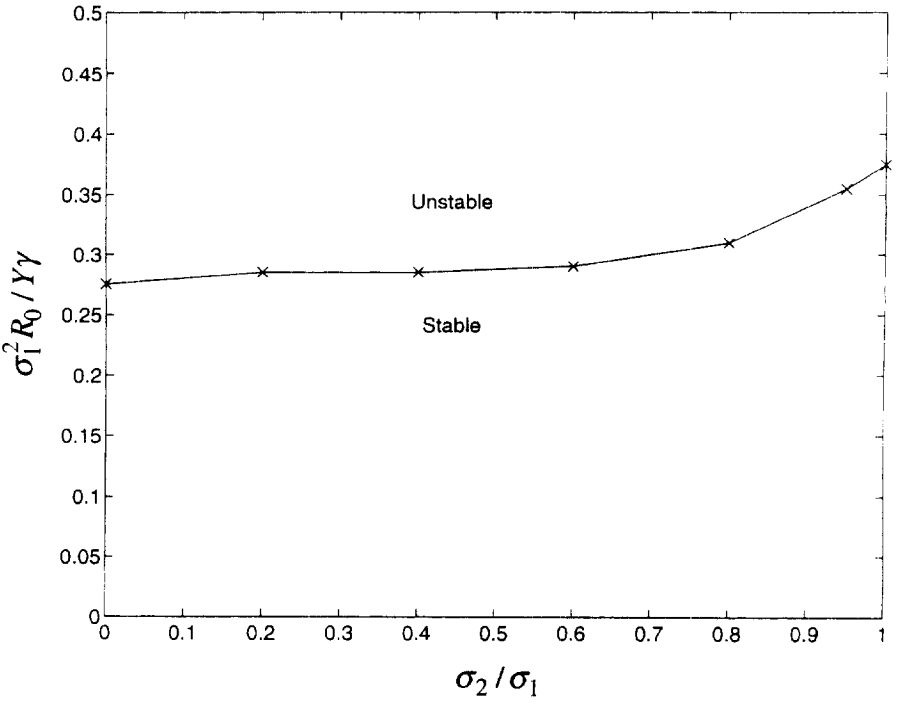

Fig. 3. The threshold of Λ as a function of the ratio of the biaxial stresses.

large, the elastic energy variation dominates, and the pore never reaches equilibrium; noses emerge at the locations transverse to the applied stress direction, and sharpen into crack tips.

We determined the critical condition by simulations at various levels of Λ, which is plotted in Fig. 3 as a function of the ratio of the applied stresses in the two directions. Below the curve, the pore is stable and does not grow crack tips; above, the pore is unstable and grows crack tips. The critical value corresponds to a threshold: a pore subject to a load below the curve has an infinite lifetime. This threshold is of great significance in designing a component to be stressed at elevated temperatures. Because the equilibrium shapes at low Λ are similar to ellipses, the curve in Fig. 3 is close to that predicted by Suo and Wang (1994) assuming that the pore evolves as a family of ellipses. The critical values of Λ vary with the applied stress states in the range

$$\frac{\sigma_1^2 R_0}{\gamma Y} \approx 0.27 \text{ to } 0.38. \tag{27}$$

For a spherical pore in a three dimensional elastic field, the calculation of Sun *et al.* (1994) showed that the threshold values are in the range 0.9 to 1.8.

5.2. *Supercritical Pores*

Next examine pores subject to loads above the threshold. Figure 4 plots the length between the pore center and a nose tip, b, as a function of time. Each curve corresponds

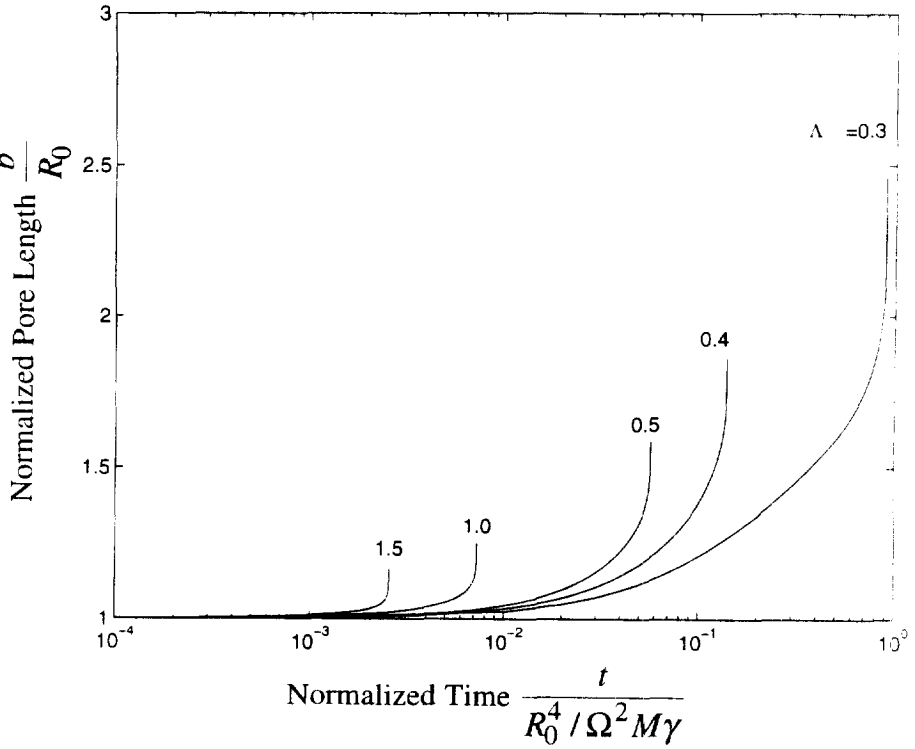

Fig. 4. The pore elongation as a function of time (uniaxial tension σ_1).

to a pore under a certain supercritical level of Λ. All pores are under a uniaxial stress, starting with a circular pore and stopping when crack tips form. The length b initially grows slowly, but accelerates as the noses sharpen. A pore under a smaller Λ grows longer noses before they become crack tips.

When a nose is nearly as sharp as a crack tip, the growth rate approaches infinity, and the mapping function ceases to be analytic at the nose tip. We stopped the simulation when $\omega'(\zeta)\to 0$ at the nose tip. Physically, the crack tip is no longer in local equilibrium. Associated with the crack advancing per unit distance, the elastic energy variation (i.e., the elastic energy release rate in the fracture mechanics), $\mathcal{G}$, exceeds the surface energy variation, 2γ. Consequently, the crack velocity cannot be limited by self-diffusion, which is the only kinetic process in our numerical simulation. To limit the crack velocity, other kinetic processes must be invoked.

In the terminology of Section 2, self-diffusion limits the stage I lifetime, t_1, namely, the time needed for a pore to grow crack tips. The values of t_1 are obtained when the curves in Fig. 4 turn vertical, and are plotted in Fig. 5 as a function of Λ, for several ratios of the applied biaxial stresses. When Λ just exceeds the threshold, t_1 is of the order of the characteristic time τ_0 defined by (26). When Λ is much above the threshold, t_1 is only a small fraction of the characteristic time τ_0. The presence of an applied stress in the nose growth direction increases t_1. This trend is readily understood by a comparison of the two limiting cases, uniaxial tension and equal biaxial tension. The

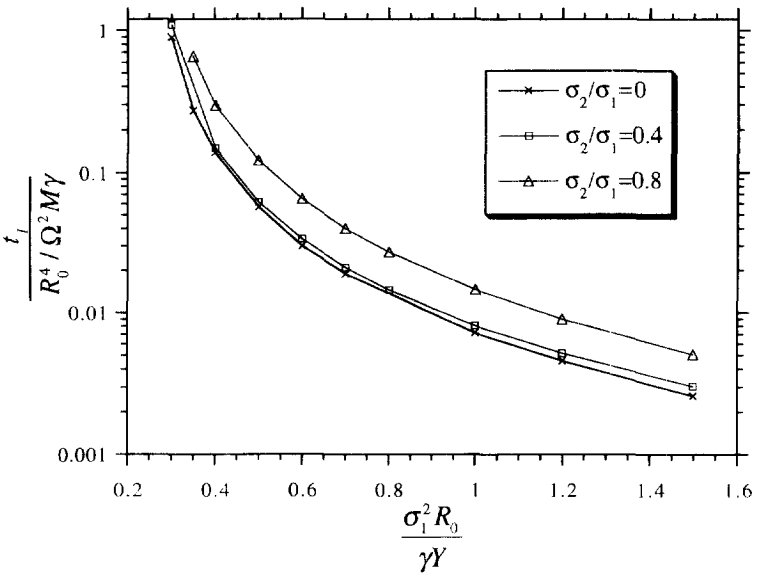

Fig. 5. The time needed for a pore to grow crack tips as a function of the applied stress.

former biases the stress distribution along the pore surface and thereby increases the rate of change. The magnitude of t_1 depends on surface diffusivity, which in turn depends exponentially on temperature.

To show the effect of the initial pore radius on t_1 under fixed applied stresses, we normalize the time by a scale independent of pore radius:

$$\tau_1 = \frac{Y^4\gamma^3}{\Omega^2 M\sigma_1^8}. \tag{28}$$

This scale relates to the one in (26) as $\tau_1 = \tau_0\Lambda^{-4}$. Figure 6 plots the normalized time for a pore to grow crack tips as a function of the normalized pore radius. When the initial pore radius just exceeds the threshold, the excess energy to drive the instability is small, and t_1 is large. When the initial pore radius is large, the diffusion length to cause the instability is long, and t_1 is also large. Consequently, everything else being fixed, a pore of an intermediate radius needs the shortest time to form crack tips. Figure 6 shows that, for example, under a uniaxial tension this radius corresponds to $\sigma_1^2 R_0/Y\gamma \approx 0.5$. When the initial radius is very large, the pore surface approaches a flat surface. The time to form a crack tip no longer depends on the pore radius, but on the initial surface imperfection (Chiu and Gao, 1993; Yang and Srolovitz, 1993). No attempt has been made to match the solution of the pore to that of a flat surface.

Denote b_1 as the distance between the pore center to the crack tip when the crack tip just forms. As is evident from Fig. 4, it is more difficult to accurately determine b_1 and t_1. Figure 7 plots b_1/R_0 as a function of Λ for several ratios of the applied biaxial stresses. When Λ just exceeds the threshold, the nose development involves overall pore shape change, resulting in a long b_1. When Λ is large, the nose development involves localized pore shape change, resulting in a short b_1. The small amount of

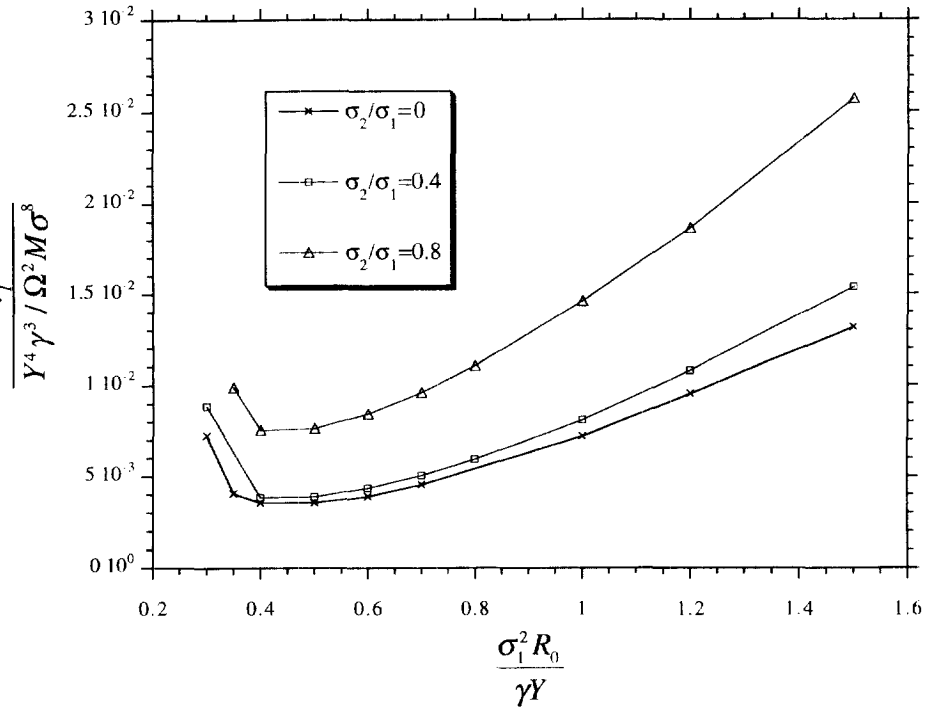

Fig. 6. The time needed for a pore to grow crack tips as a function of the initial pore radius.

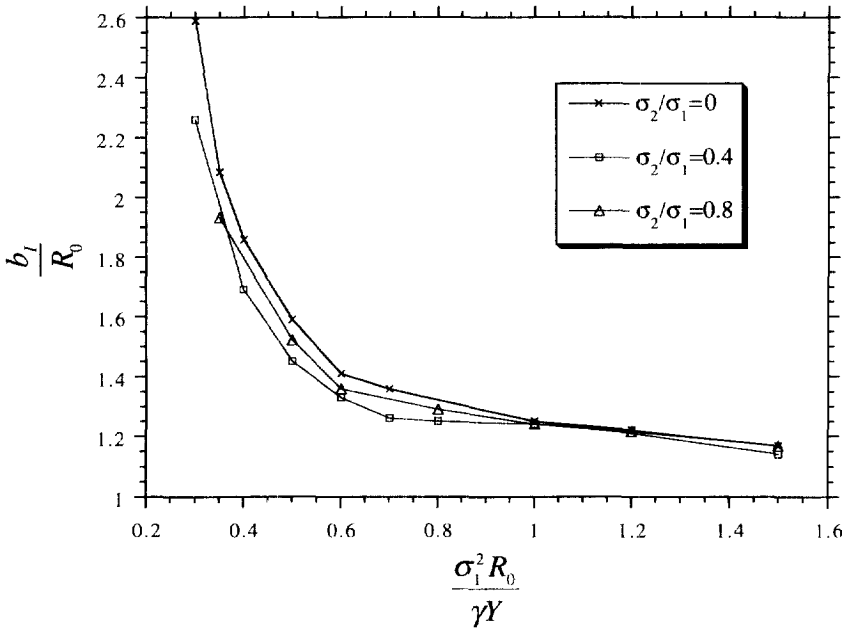

Fig. 7. The length of the crack when it just forms by surface diffusion.

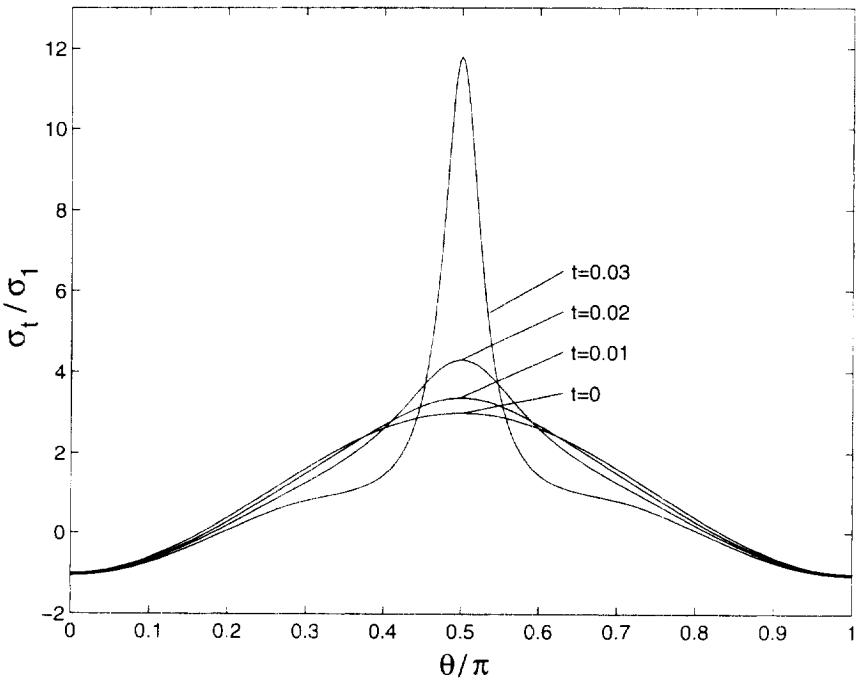

Fig. 8. The distribution of the hoop stress on the pore surface at various times ($\Lambda = 0.6$, uniaxial tension σ_1).

geometric change, however, need not imply that the time to grow the crack tips contributes insignificantly to the total lifetime, as discussed in Section 1. Also observe that b_1 is insensitive to the applied stress state.

5.3. *Stress concentration*

Figure 8 plots the hoop stress, σ_t, on the pore surface at various times. The loading condition is the same as that in Fig. 2(b) (uniaxial tension, $\Lambda = 0.6$). The upper half of the unit circle on the ζ-plane, $0 \leqslant \theta \leqslant \pi$, maps to the upper half of the pore surface. In the beginning, the circular pore has stress concentration factor 3, in agreement with the classical elasticity solution. After the nose emerges, the stress concentrates more. As the nose sharpens to become a crack tip, the stress field is square root singular. At a distance r ahead of a opening crack tip, the stress normal to the crack tales the well-known asymptotic form, $K(2\pi r)^{1/2}$, where K is the stress intensity factor. In the simulation, we computed the stress directly ahead of the crack tip, and extracted the K value according to the asymptotic form. The elastic energy variation associated with the crack advancing per unit distance, $\mathcal{G}$, relates to the stress intensity factor by Irwin's relation, $\mathcal{G} = K^2/Y$. Figure 9 plots the energy release rate when the crack just forms. When Λ just exceeds the threshold, $\mathcal{G}$ is slightly above $2\gamma_s$ — that is, the crack tip is nearly in local equilibrium, and approximately satisfies the Griffith condition. When Λ is much above the critical value the crack tip is not in local equilibrium. The shape change is localized and can be approximated by cracks connected to a circular

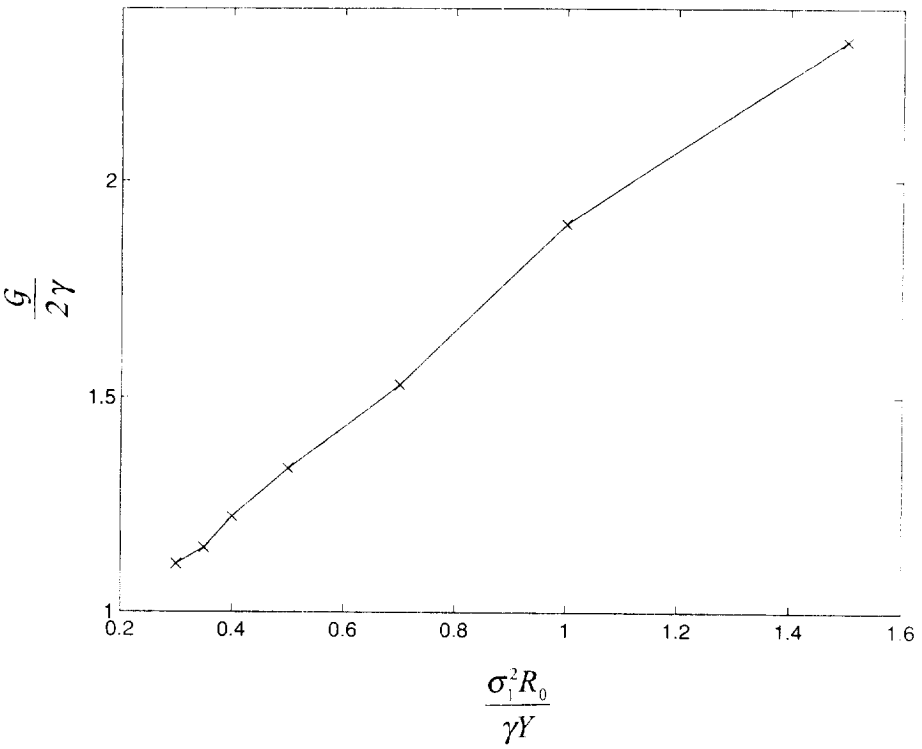

Fig. 9. The energy release rate as a function of Λ.

hole. The stress intensity factor for the latter is available (Tada *et al.*, 1985). Figure 10 compares the stress intensity factors for the two geometries.

5.4. *Surface tension anisotropy*

All the above simulations assumed that surface tension is isotropic. We next explore the effect of surface tension anisotropy by assuming that the surface tension varies with the crystal orientation according to

$$\gamma = \gamma_0(1 + g\sin^2\beta). \tag{29}$$

With reference to Fig. 1, β is the angle from the x-axis to the surface normal, γ_0 the surface tension of the crystal plane normal to the x-axis, and g a parameter indicating the extent of anisotropy. The total surface energy, U_S, is the integral of γ over the pore surface. We use γ_0 in various dimensionless groups introduced above.

Sun *et al.* (1994) used the same anisotropic function and showed that g affects the threshold value of Λ. Here we concentrate on supercritical pores. In the present simulation, we started with a circular pore and allowed it to approach its equilibrium shape under the influence of the surface tension anisotropy, with no applied stress. Typically, after a time on the order of τ_0, the pore is close to the equilibrium shape and does not change shape appreciably any more. We then applied the stresses to

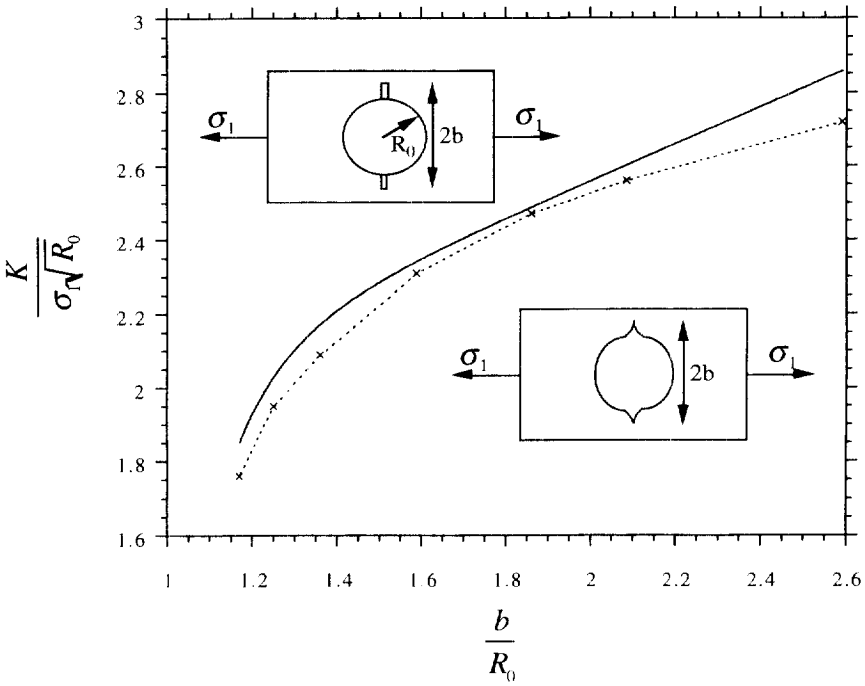

Fig. 10. A comparison of the stress intensity factor between a crack grown from a nose and a crack connected to a circular hole.

further change the pore shape. Figure 11 shows t_1 and b_1 as functions of g (uniaxial tension, $\Lambda = 0.4$). When $g > 0$, the crystal surface normal to the x-axis has the smallest surface tension, so that the anisotropy favors a pore elongating transverse to the loading direction and thereby decreases t_1 and b_1. The converse is true when $g < 0$. Everything else being fixed, surface tension anisotropy can change t_1 by orders of magnitude for a pore near the threshold.

When g is large, the Wulff construction shows that a pore forms two cusps even before the stress is applied. Figure 12 shows that the pore relaxed from our simulation (b) is very close to that obtained from the Wulff construction (a). Under an applied stress, the cusp sharpens into a crack (c).

6. SUMMARY OF RESULTS

We assume that the fracture of a crystal stressed in tension at a high temperature takes the following steps. A rounded pore first changes shape to grow crack tips, the rate of which is limited by surface diffusion. After the crack tips form, they extend by slow decohesion, followed by fast fracture. This paper studies in some detail the pore shape change process. A pore can grow crack tips when the parameter Λ exceeds a threshold. Below it, the pore reaches an equilibrium shape without forming crack tips. The time for a supercritical pore to grow crack tips depends on the loading level,

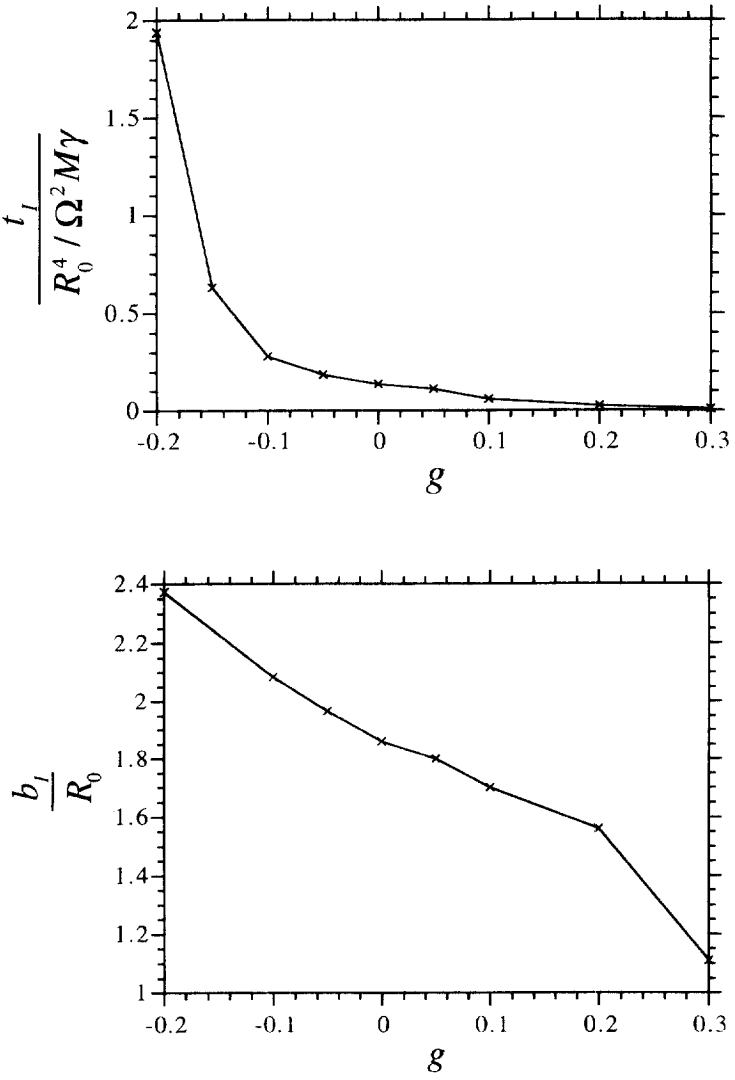

Fig. 11. The effect of surface tension anisotropy on the time for a pore to grow crack tips and the crack length when it just forms ($\Lambda = 0.4$, uniaxial tension σ_1).

the applied stress state, and surface tension anisotropy. When a supercritical pore forms crack tips, the crack tips are not in local equilibrium, and the crack velocity is not limited by surface diffusion. The stress intensity factor at a crack tip grown from a nose is well approximated by a crack connected to a circular hole.

ACKNOWLEDGEMENTS

The work was supported by ARPA through a URI contract N-0014-92-J-1808, and by NSF through grant MSS-9202165. Professor T. H. Hao contributed in the early stage of this work.

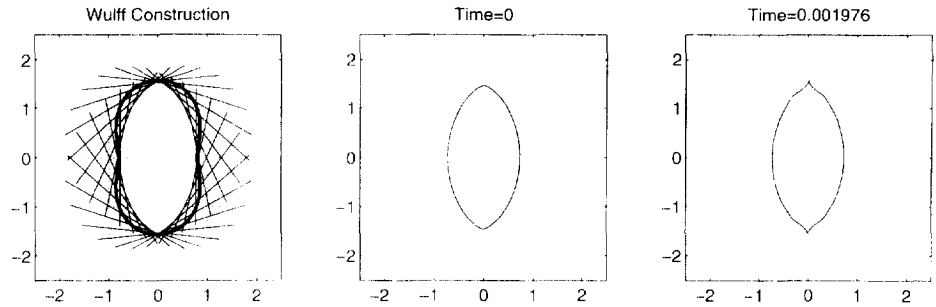

Fig. 12. (a) Even when no stress is applied, highly anisotropic surface tension ($g = 1$) gives rise to cusps on the equilibrium pore surface, as determined by the Wulff construction. (b) The same equilibrium pore shape determined by the dynamical simulation after relaxation under no stress. (c) Sharp noses emerge under the uniaxial tension σ_1 at $\Lambda = 0.6$.

REFERENCES

Asaro, R. J. and Tiller, W. A. (1972) Interface morphology development during stress corrosion cracking: Part I. Via surface diffusion. *Metall. Trans.* **3,** 1789–1796.

Budiansky, B., Hutchinson, J. W. and Slutsky, S. (1982) Void growth and collapse in viscous solids. *Mechanics of Solids, The Rodney Hill 60th Anniversary Volume*, ed. H. G. Hopkins and J. Sewell, pp. 13–45. Pergamon Press, Oxford.

Chiu, C. H. and Gao, H. (1993) Stress singularities along a cycloid rough surface. *Int. J. Solids Structures* **30,** 2981–3012.

Chuang, T.-J., Kagawa, K. I., Rice, J. R. and Sills, L. B. (1979) Non-equilibrium models for diffusive cavitation of grain interfaces. *Acta Metall.* **27,** 265–284.

Freund, L. B. and Jonsdottir, F. (1993) Instability of a biaxially stressed thin film on a substrate due to material diffusion over its free surface. *J. Mech. Phys. Solids* **41,** 1245–1264.

Gao, H. (1991) A boundary perturbation analysis for elastic inclusions and interfaces. *Int. J. Solids Structure* **28,** 703–725.

Gao, H. (1992) Stress analysis of holes in anisotropic elastic solids: conformal mapping and boundary perturbation. *Q. J. Mech. Appl. Math.* **45,** 149–168.

Gao, H. (1995) The hypocycloid cavity: a path from a Griffith slit crack to a cusped cycloid surface. *Proc. Roy. Soc. Lond.* **448,** 465–483.

Grinfeld, M. (1986) Instability of the separation boundary between a nonhydrostatically stressed elastic body and melt. *Sov. Phys. Dokl.* **31,** 831–834.

Hull, D. and Rimmer, D. E. (1959) The growth of grain-boundary voids under stress. *Phil. Mag.* **4,** 673–687.

McCartney, L. N. (1977) Cavities under stress at high temperatures. *Acta Metall.* **25,** 221–230.

Newcomb, S. A. and Tressler, R. E. (1993) Slow crack growth in sapphire fibers at 800 to 1500 C. *J. Am. Ceram. Soc.* **76,** 2505–2512.

Rice, J. R. and Chuang, T.-J. (1981) Energy variations in diffusive cavity growth. *J. Am. Ceram. Soc.* **64,** 46–53.

Schowalter, L. J. (1996) Heteroepitaxy and strain, *MRS Bulletin*, April.

Spencer, B. J., Voorhees, P. W. and Davis, S. H. (1991) Morphological instability in epitaxially strained dislocation-free solid films. *Phys. Rev. Lett.* **67,** 3696–3699.

Srolovitz, D. J. (1989) On the stability of surfaces of stressed solids. *Acta Metall.* **37,** 621–625.

Stevens, R. N. and Dutton, R. (1971) The propagation of Griffith cracks at high temperatures by mass transport processes. *Mater. Sci. Engng* **8,** 220–234.

Sun, B., Suo, Z. and Evans, A. G. (1994) Emergence of crack by mass transport in elastic crystals stressed at high temperatures. *J. Mech. Phys. Solids* **42,** 1653–1677.

Suo, Z. and Wang, W. (1994) Diffusive void bifurcation in stressed solid. *J. Appl. Phys.* **76,** 3410–3421.

Tada, H., Paris, P. C. and Irwin, G. R. (1985) *Stress Analysis of Cracks Handbook*. Paris Productions Inc., St. Louis, Missouri.

Wang, W. Q., Suo, Z. and Hao, T.-H. (1996) A simulation of electromigration-induced transgranular slits. *J. Appl. Phys.* **79,** 2394–2403.

Wong, D. and Thouless, M. D. (1996) Effects of elastic relaxation on aspect ratios during island growth of isotropic films. Submitted for publication.

Yacobson, B. I. (1993) Stress-promoted interface diffusion as a precursor of fracture. *J. Chem. Phys.* **99,** 6923–6934.

Yang, W. H. and Srolovitz, D. J. (1993) Cracklike surface instabilities in stressed solids. *Phys. Rev. Lett.* **71,** 1593–1596.